Predictive Model for Thermal and Stress Field in Selective Laser Melting Process -- Part I

Lan Li

Lei Yan

Wenyuan Cui

Yitao Chen

et. al. For a complete list of authors, see *https://scholarsmine.mst.edu/mec_aereng_facwork/4477*

Recommended Citation

25th International Conference on Production Research Manufacturing Innovation:
Cyber Physical Manufacturing
August 9-14, 2019 | Chicago, Illinois (USA)

Predictive Model for Thermal and Stress Field in Selective Laser Melting Process—Part I

Lan Li*, Lei Yan, Wenyuan Cui, Yitao Chen, Tan Pan, Xinchang Zhang, Aaron Flood, Frank Liou

Missouri University of Science and Technology, 205 W 12th St, Rolla, MO, 65401, USA

Abstract

During the part forming in laser powder bed fusion process, thermal distortion is one big problem due to the thermal stress which is caused by the high cooling rate and temperature gradient. Therefore, it is important to know the effect of process parameters on thermal and stress evolution in the melt zone. In this paper, a 3D finite element model for Selective Laser Melting (SLM) process based on sequentially coupled thermo-mechanical field analysis was developed for accurately predicting thermal history and surface features, like distortion and residual stress. Temperature dependent material properties for performed material 304L stainless steel are incorporated into the model capturing the change from powder to fully dense solid stainless steel. Surface temperature gradients and thermal stress were fully presented in the development of different parameter sets, which designed for the probability of reducing defect formation. Simulation results showed that the sequent thermal cyclic melting in successive scanned tracks resulted in alternating compressive and tensile thermal stresses. A predictive model for thermal and stress field in large part by selective laser melting process is come up in Part II. After the parts cooled down to room temperature, higher residual stresses were found in longitudinal stress. This paper will provide guidance on how to achieve minimum residual stresses and deformations by the study of the process parameters.

Keywords: SLM; finite element analysis; distortion; residual stress

* Corresponding author. Tel.: +1-573-612-9152
E-mail address: ll752@mst.edu

1. Introduction

Selective Laser Melting (SLM) is a powder bed-based Additive Manufacturing (AM) technology. It is widely used in the freeform fabrication of complex three-dimensional metal parts directly from CAD models by adding material layer by layer [1]. SLM introduces the opportunity to build parts with high engineered properties. However, several process defects such as warping and distortion, induced by residual stress, have been discovered in the SLM process. Residual stresses generate due to the high thermal

gradient during rapid heating and cooling cycles of the part forming in laser powder bed fusion. These process defects still remain unsolved issues [2]. Therefore, it is critical to understand how SLM process parameters such as laser power, scanning speed and scanning strategy determine the thermal behavior and mechanical properties of the final parts. However, it is time-consuming and highly cost through experiments for detailed investigations to analyze the effect of different process parameters on the temperature distribution and mechanical properties. This problem can be solved by developing a numerical model to analyze all behaviors in the SLM process and understand how process parameters relate to the thermal behavior and ultimate engineering mechanical properties.

In recent years, numerical models have been developed and used in previous studies to analyze the relations between process parameters and mechanical performance [3-5]. Antony et al. [6] conducted a numerical and experimental work on selective laser melting process performed with the material of 316L stainless steel. They analyzed the effect of process parameters such as laser power, scanning speed and laser beam size on melt pool sizes and ball formation. Conclusions were included that scanning speed had no influence on track height and wetting angle, while laser power and scanning speed had obvious effects on track smoothness, distortion and irregularities. These simulation results were compared with experimental results. Parry et al. [7] developed a thermo-mechanical model to determine the thermal behavior and residual stress resulting from the SLM process. They found that scan strategies affected the stress distribution. Their results showed longitudinal stress was the main contribution to stress due to the larger thermal gradient in the laser scanning direction. It was also believed that preheating temperature affected thermal stress and cracks significantly [8]. For example, Cao et al. [9] established a three-dimensional thermo-mechanical model to analyze the effect of preheating on stress and distortion in electron beam based additive manufacturing, their results indicated that preheating could decrease the distortion and stress of final parts.

In this paper, a 3D finite element model for SLM process with the performed material of SS304L based on sequentially coupled thermo-mechanical field analysis in commercial software ANSYS was developed for accurately predicting thermal history, distortion and residual stress. Temperature dependent material properties were incorporated into the model capturing the change from powder to fully dense solid stainless steel. For the sequentially coupled thermo-mechanical analysis, the calculations were done in two steps. First, the transient thermal analysis was calculated. Then the computed temperature results were used for the mechanical calculations as the thermal load to calculate the thermal stress and deformation. Simulation results showed that the sequent thermal cyclic melting in successive scanned tracks resulted in alternating compressive and tensile thermal stresses. This paper will provide guidance on how to achieve minimum residual stresses and deformations by controlling the process parameters and other relevant parameters.

2. Numerical analysis of selective laser melting 304L stainless steel

2.1. Model setup

The three-dimensional numerical modeling domain was setup by one layer of 304L stainless steel powder with dimensions of $4 \times 3.4 \times 0.05$ mm³ on a solid 304L substrate with dimensions of $4 \times 3.4 \times 2$ mm³ (Fig. 1). To reduce computational time, the elements interacting with the laser beam were finely meshed with hexahedral element sizes of 20 µm and a coarser mesh for the surrounding loose powder and substrate. The final model contained total 45,168 elements and 54469 nodes. In order to make the complicated problem mathematically tractable, the whole powder bed was considered as homogeneous and continuous media.

2.2. Governing equations for heat transfer and thermal stress

The governing transient heat transfer energy balance equation in the entire volume of the material is given as

$$\rho c_p \frac{\partial T}{\partial t} = \frac{\partial}{\partial x}(k \frac{\partial T}{\partial x}) + \frac{\partial}{\partial y}(k \frac{\partial T}{\partial y}) + \frac{\partial}{\partial z}(k \frac{\partial T}{\partial z}) + \dot{q} \tag{1}$$

where k is the thermal conductivity, ρ is the density, c_p is the specific heat, both of the thermal conductivity and thermal diffusivity are temperature dependent, T is the current temperature, $\dot{q}$ is the internal heat generation rate per unit volume, t is the time, x, y and z are the coordinates in the reference system.

For the sequentially coupled thermo-mechanical analysis. The calculations are done in two steps [10]. First, the transient thermal analysis is calculated. After the temperature field obtained from the thermal analysis, the mechanical analysis is performed as the temperature field applied as the thermal load to calculate the thermal stress and deformation.

The governing mechanical equilibrium equation is written as [11-12]:

$$\nabla \cdot \sigma = 0 \tag{2}$$

where σ is the second-order stress tensor associated with the material behavior law.
Considering the elastoplastic behavior of the material, strain and stress can be written as

$$\sigma = C\varepsilon^e \tag{3}$$

where C is the fourth order material stiffness tensor and ε^e is the second-order elastic strain tensor.

Total strain ε, assuming small deformation thermo-elasto-plasticity, is decomposed as [13]:

$$\varepsilon = \varepsilon^e + \varepsilon^p + \varepsilon^{th} + \varepsilon^v \tag{4}$$

where ε^e, ε^p, ε^{th} and ε^v are the elastic strain, plastic strain, thermal strain and transformation strain, respectively.

2.3. Heat source model and boundary conditions

During the SLM process, the laser energy on the powder bed can be regarded as a volumetric energy density, which obeys the Gaussian heat source distribution. The most common beam profile in the laser material processing is the Gaussian distribution with an exponentially decaying of energy as a volumetric heat source given by:

$$\dot{q}_1 = \frac{2(1-R)P}{\pi r_0^2 d} \exp\left[-2\frac{r^2}{r_0^2}\right] \cdot \exp\left[-\frac{z}{d}\right] \tag{5}$$

where P is the laser power, r_0 is the laser radius, d is the optical penetration depth, which is set as 50 μm in this work. Eq.(5) creates an exponentially decaying volumetric heat flux through a Gaussian distribution in the (x, y) plane and an additional decay term in the z direction.

The initial condition throughout the whole powder bed and substrate is considered as uniform temperature distribution:

$$T(x, y, z, t)_{t=0} = T_0 \tag{6}$$

where T_0 is the ambient temperature which equals the temperature at the initial time.

Boundary conditions on the top surface and lateral surfaces include radiation and convection. Boundary conditions are expressed as:

$$\ddot{q} = -k\frac{\partial T}{\partial z} + h(T - T_0) + \varepsilon\sigma(T^4 - T_0^4) \tag{7}$$

where T is temperature, h is the heat transfer coefficient of natural thermal convection, which is assumed to be a constant of 50 W/m²·K, σ is the Stefan‐Boltzmann constant of 5.67×10^{-8} W/m²·K⁴ and ε is the powder bed emissivity of 0.4.

The laser beam scans the powder bed back and forth with the hatch space of 105 μm at a constant effective scanning velocity along the X-direction. Other process parameters of the simulation model of 304L stainless steel are shown in Table 1.
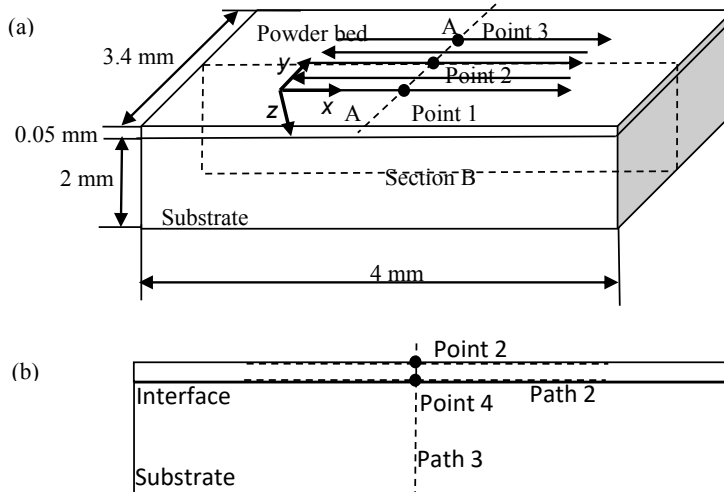

Fig. 1. (a) FEA model geometry and laser scan strategy of SLM process; (b) longitudinal view of middle section B

Another boundary condition specifies that there is no heat exchange at the bottom surface of the substrate, which means the bottom surface is adiabatic. Usually, all nodes at the bottom region are rigidly constrained as no deformation occurred during the SLM process [14].

For the sequentially coupled thermo-mechanical analysis, the calculations were done in two steps. First, the transient thermal analysis was calculated. Then the computed temperature results were used for the mechanical calculations as the thermal load to calculate the thermal stress and deformation. The first step was the heating process which lasted 0.00625 s and cooling process which lasted 50 s. During this process, the powder is heated by the moving laser beam and then cools down to the room temperature.

Table 1. Hatch parameters of the simulation model

Hatch parameters	Model
Power, P [W]	200
Optical penetration depth, d [μm]	50
Hatch spacing, Hs [μm]	105
Point distance, pd [μm]	60
Laser exposure time, t_e [μs]	75
Effective scan speed, SS [mm/s]	800
Laser diameter, D [μm]	150
Reflectance of SS304L, R	0.3
Number of laser tracks, N	5

2.4. Thermo-physical and mechanical properties

The thermo-physical properties and mechanical properties of solid-state 304L stainless steel are temperature dependent and identified in [15-16].

Thermal conductivity in this work is assigned an increased value 10 times the normal thermal conductivity of solid 304L for temperature greater than the melting point. The value of thermal conductivity multiplier was determined through fitting the model's predicted melt pool size to experimental results. This method of effective thermal conductivity of the melt pool is well established in other literature and is used to simulate the increased heat transfer due to convection of the melt pool in conduction models [17]. The effective properties of the powder bed are much smaller than that of bulk material, for the used powder material in this study, expressed as in paper [18]. We can tread the yield stress and Young's Module as zero in powder.

Table 2. Thermo-physical properties and mechanical properties of solid state SS304L

T(K)	c_p(J/(kg·K))	k(W/(m·K))	ρ(kg/m³)	H(kJ)	σ_y(MPa)	α(K⁻¹)	E(GPa)	v
298	480	14.8	8020	0	220	2.00E-05	200	0.3
373	500	15.8	8000	36	218	2.00E-05	193	0.3
473	530	17.7	7950	88	186	2.00E-05	185	0.3
573	540	18.8	7903	141	170	2.00E-05	175	0.3
673	560	20.7	7855	196	155	2.00E-05	165	0.3
873	595	23.5	7751	311	145	2.00E-05	160	0.3
1073	620	25.8	7645	432	91	2.00E-05	150	0.3
1473	675	31.6	7431	690	25	2.00E-05	60	0.3
1573	695	32.8	7381	758	21	2.00E-05	20	0.3
1673	720	33.5	7351	801	20	2.00E-05	10	0.3
1727	800	140	6900	1129	10	2.00E-05	10	0.3
1773	800	300	6900	1166	10	2.00E-05	10	0.3
1873	800	300	6900	1246	10	2.00E-05	10	0.3

Taking the melting and solidification phenomena during SLM into consideration, the latent heat of fusion should not be neglected. It can be calculated from the enthalpy (*H*) of the material, which can be written as [19]:

$$H(T) = \begin{cases} \int \rho c_p dT, & T < T_s \\ \int \rho c_p dT + \rho \dfrac{T - T_s}{T_l - T_s} \cdot L, & T_s \leq T \leq T_l \\ \int \rho c_p dT + \rho L, & T > T_l \end{cases} \tag{8}$$

where *L,* 261 kJ/kg, is the latent heat of fusion, T_l, 1727 K and T_s, 1673K are the liquidus and solidus temperature, respectively [15].

3. Simulation Results and Discussion

Fig. 2 (a) shows the computed temperature profile changes at various monitoring locations, points 2, 4, 5 and 6 for a laser power of 200 W, as from Figure 1. Point 2 is in the middle of the third track on the top surface; Point 4 is below Point 1 and located at the interface of powder bed and substrate; Point 5 and 6 are in the middle of the second and fourth track on the top surface. Results indicate that during the heating process, the heating rate is very fast. Each point experiences several peak temperatures due to heat accumulation from sequent laser tracks. The lower secondary peaks correspond to the laser scanning the middle position on successive tracks. For example, there are several peak temperatures in Point 2. The maximum peak temperature is higher than the melting temperature, and two sequent secondary peaks are a litter lower than the melting temperature. This means point 2 is affected by several tracks, but no re-melting happens by the two adjacent tracks. The thermal history and simulated melt pool sizes are obtained and validated by the solidification behavior in paper [20]. In this paper, the melt pool depth is larger than the layer thickness of 50 μm, which means thermal behavior of the previous layer can also be affected by laser tracks on the subsequent layer. Even re-melting happens when heating a subsequent layer.
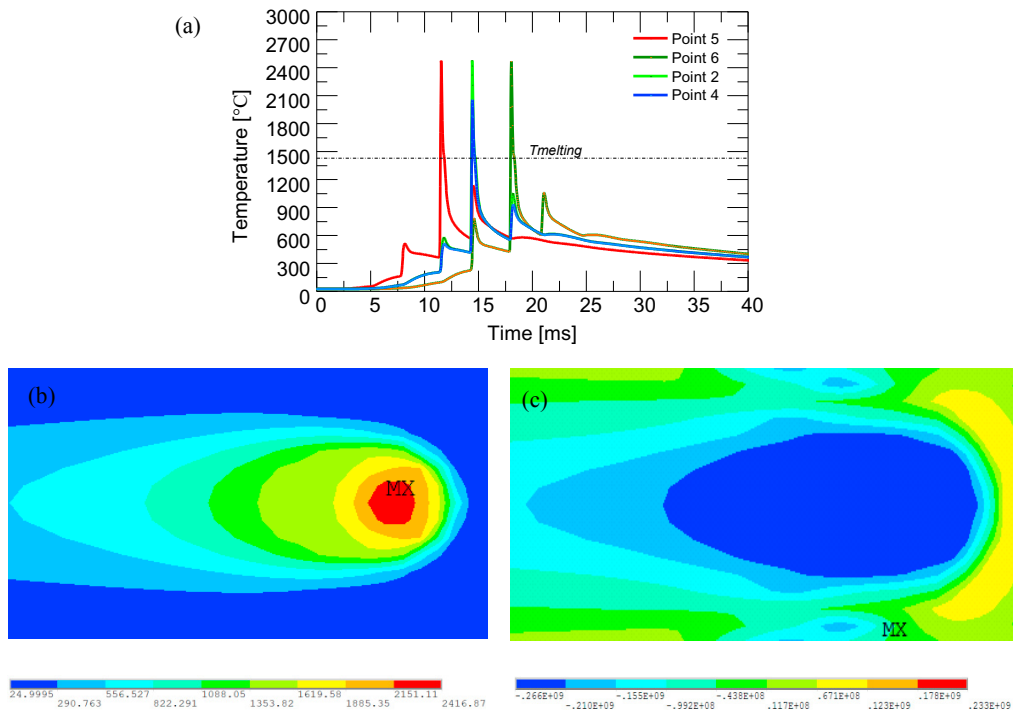

Fig. 2. (a) Thermal history of Points 2-6 for laser power of 200 W, (b) temperature distribution profile when laser travels in point 1 and (c) thermal stress corresponding to (b).

Fig. 2 (b) shows the temperature profile contour in laser track when laser travels in point 1, the middle of the first track. The temperature change of the distribution indicates the temperature gradient of the melting regions becomes steeper as distance with laser center increases, which indicates temperature gradient and cooling rate increase when distance into the melt region center increases. It is noted that the temperature gradient becomes higher when laser power increases. Thus, the process with a higher laser power of 200W generates higher temperature gradient. Actually, the larger temperature gradient induces higher stress, which means a higher laser power will induce a greater residual stress field within alloys part.

In the laser heating process, the outer region is cooler than the laser center; therefore outer region tends to contract before the center region, so the outer region experiences tension, while the center regions find themselves in compression. This can be verified in Figure 2 (c), the center regions have a higher temperature and even higher than the melting point, then the equivalent stress remains in compressive compared to the outer space. It is noting that the evolution of stress is dependent on the direction of local thermal gradients. After cooling is completed, the material surface remains in compression, with the inner sustains tension.

The typical point is selected in Point 2, the middle of the third track. The stress variation and history are illustrated in Figure 3 (a) and (b). The stress in longitudinal, transversal, normalized direction and von Mises stress are observed respectively. Obviously, different stress directions presented the complicated variation trend in the laser heating process. Then reach a constant value eventually as the part cools down to room temperature. The values of final residual stress in different directions were found, with the value of X-component stress 98 MPa, Y-component stress 26 MPa, Z-component stress 12 MPa and von Mises stress 127 MPa, respectively. These results show that longitudinal stress is the main contribution to stress due to the larger thermal gradient in the laser scanning direction.

The thermal stress history of different directions during heating period (0–0.006250 s) are shown in Figure 3 (b). It is worth noting that the value of the thermal stress is negative at the beginning of the heating process, which meant that the stress is in compressive state. As the heating process proceeds, the compressive stress decreases rapidly and turns into tensile state [21]. Because of the remelting between adjacent scan tracks happens at successive scanning tracks, the variations of the stresses are complicated as the laser heat source moves rapidly. The subsequent thermal cyclic melting in successive scanned tracks result in alternating compressive and tensile thermal stresses.
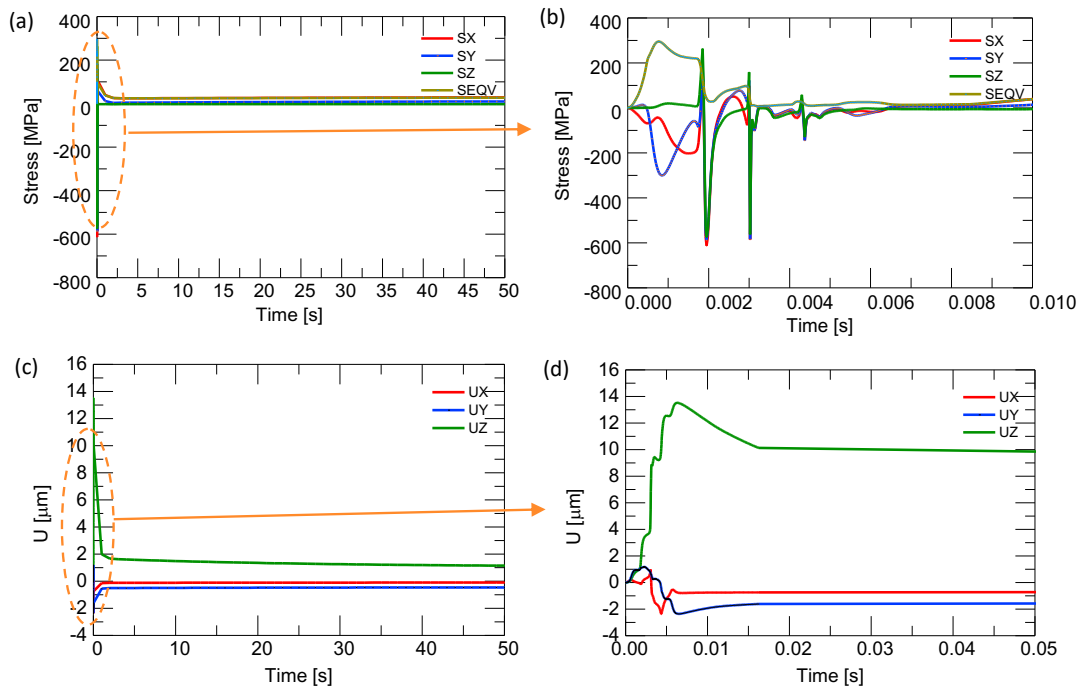

Fig. 3. The different stress distributions and different deformation distributions of middle point on the third track: The different stress distributions during the whole simulated time (a) (b); The different deformation distributions during the whole simulated time (c)(d).

The deformation distributions in Point 2 are illustrated in Figure 3 (c) and (d). The deformation in longitudinal, transversal and normalized direction are observed respectively. Like the stress variation history, different deformation directions present the complicated variation trend in the laser heating process. Then reach a constant value eventually as the part cools down to room temperature. The values of final deformation in different directions are found, with the value of X-component -0.13 μm, Y-component -0.00005 μm and Z-component 0.55 μm, respectively. Another thing that is worth noting is that maximum deformation in the normalized direction (z direction) is higher than that in x and y direction. The peak value of deformation in the normalized direction (z direction) is about 14 μm.

Conclusions

A 3D coupled thermo-mechanical field analysis FEA model of single-layer multi-track SLM component was conducted and the temperature history and the thermal stress were analyzed. Following conclusions can be drawn from the study:

(1) For thermal history, each point experiences several peak temperatures due to heat accumulation from sequent laser tracks. While the successive tracks are scanned using shorter track passes compared with the long and numerous tracks when building large part, it results in more localized thermal gradients.

(2) Thermal cyclic melting in successive scanned tracks results in alternating thermal stresses. Different stress and deformation component cycles present the complicated variation trend in the laser heating process. Then reach a constant value eventually as the part cools down to room temperature.

(3) At the selecting typical point, longitudinal stresses are larger compared to the normal and transverse stresses. While for the deformation, the value of normal direction is higher than the other two directions.

Because of the small dimension of the simulated part, extra stress could be caused by localized yielding with localized thermal gradients in a small simulated part. Therefore, the residual stress of the large part is necessary to analyze. Moreover, a practical part may require hundreds or thousands of layers in SLM and dramatically increases the computational time. A predictive model for thermal and stress field in large part by selective laser melting process is come up in Part II.

Acknowledgements

References

[1] Patil, R. B., Yadava, V., 2007, Finite element analysis of temperature distribution in single metallic powder layer during metal laser sintering, Int. J. Mach. Tools Manuf., 47(7–8), pp. 1069–1080.

[2] Zhibo Luo, Yaoyao Zhao, A survey of finite element analysis of temperature and thermal stress fields in powder bed fusion Additive Manufacturing, Additive Manufacturing, Volume 21, May 2018, Pages 318-332.

[3] A.S. Wu, D.W. Brown, M. Kumar, G.F. Gallegos, W.E. King, An experimental investigation into additive manufacturing-induced residual stresses in 316L stainless steel, Metall. Mater. Trans. A 45 (2014) 6260–6270.

[4] H.H. Zhao, G.J. Zhang, Z.Q. Yin, L. Wu, A 3D dynamical analysis of thermal behavior during single-pass multi-layer weld-based rapid prototyping, J. Mater. Process. Technol., 211 (2011), pp. 488-495.

[5] J. Ding, P. Colegrove, J. Mehnen, S. Ganguly, P.M.S. Almeida, F. Wang, S. Williams, Thermo-mechanical analysis of wire and arc additive layer manufacturing process on large multi-layer parts, Comput. Mater. Sci., 50 (2011), pp. 3315-3322.

[6] Antony, K., Arivazhagan, N., and Senthilkumaran, K., 2014, "Numerical and experimental investigations on laser melting of stainless steel 316L metal powders," J. of Man. Proc., 16(3), pp. 345–355.

[7] Parry, L., Ashcroft, I.A., and Wildman, R.D., 2016, "Understanding the effect of laser scan strategy on residual stress in selective laser melting through thermo-mechanical simulation," Add. Man. A, 12, pp. 1–15.

[8] T. Mukherjee, J. S. Zuback, W. Zhang, T. DebRoy, 2018, "Residual stresses and distortion in additively manufactured compositionally graded and dissimilar joints," Computational Materials Science Volume 143, 15, Pages 325-337.

[9] J. Cao, M.A. Gharghouri, P. Nash, Finite-element analysis and experimental validation of thermal residual stress and distortion in electron beam additive manufactured Ti-6Al-4V build plates, J. Mater. Process. Technol., 237 (2016), pp. 409-419.

[10] H. Liu, T.E. Sparks, F.W. Liou, and D. M. Dietrich, "Numerical Analysis of thermal stress and deformation in Multi-Layer Laser Metal Deposition Process", Proceedings of 24th Solid Freeform Fabrication Symposium, Austin, TX, August 12-14, 2013.

[11] M. Megahed, H.-W. Mindt, N. N'Dri, H. Duan, O. Desmaison, Metal additive manufacturing process and residual stress modeling, Integrat. Mater. Manuf. Innov. 5 (2016) 1–33.

[12] P. Peyre, P. Aubry, R. Fabbro, R. Neveu, A. Longuet, Analytical and numerical modelling of the direct metal deposition laser process, J. Phys. D Appl. Phys. 41(2018)025403.

[13] Jeff Irwin, P. Michaleris , A Line Heat Input Model for Additive Manufacturing, J. Manuf. Sci. Eng 138(11), 111004 (Jun 23, 2016).

[14] L. Papadakis, A. Loizou, J. Risse, S. Bremen, J. Schrage, a computational reduction model for appraising structural effects in selective laser melting manufacturing: a methodical model reduction proposed for time-efficient finite element analysis of larger components in selective laser melting, Virtual Phys. Prototype. 9 (2014)17-25.

[15] Mills, K. C., 2002, Recommended Values of Thermophysical Properties for Selected Commercial Alloys, Woodhead Publishing.

[16] Dean Deng, Hidekazu Murakawa ,Numerical simulation of temperature field and residual stress in multi-pass welds in stainless steel pipe and comparison with experimental measurements, Computational Materials Science, Volume 37, Issue 3, September 2006, Pages 269-277.

[17] Ladani, L., Romano, J., Brindley, W., and Burlatsky, S., 2017, "Effective liquid conductivity for improved simulation of thermal transport in laser beam melting powder bed technology," Add. Man., 14, pp. 13–23.

[18] Zhidong Zhang, Yuze Huang, Adhitan Rani Kasinathan, Shahriar Imani Shahabad, Usman Ali, Yahya Mahmoodkhani, Ehsan Toyserkani, 3-Dimensional heat transfer modeling for laser powder-bed fusion additive manufacturing with volumetric heat sources based on varied thermal conductivity and absorptivity, Optics & Laser Technology, Volume 109, January 2019, Pages 297-312.

[19] E. Haque, P. Hampson, Modelling phase change in a 3D thermal transient analysis, Int. J. Multiphys. 8 (2014) 49–68.

[20] Li, L., Lough, C., Replogle, A., Bristow, D., Landers, R., & Kinzel, E. (2017), Thermal Modeling of 304L Stainless Steel Selective Laser Melting. Solid Freeform Fabrication, Vol. 6061, pp. 1068-1081.

[21] B. Vrancken, V. Cain, R. Knutsen, J.V. Humbeeck Scr. Mater., 87 (2014), pp. 29-32.